Brecciation of glacially overridden palaeokarst (Lower Aare Valley, northern Switzerland): result of subglacial water-pressure peaks?

Water pressures at the base of active glacial overdeepenings are known to fluctuate strongly on various timescales. Rapid peaks in basal water pressure can lead to fracturing of the glacier bed, a process that has been described at numerous sites around the world, mostly based on large hydrofracture systems. This article presents drill cores from the base of a >100 m deep glacial overdeepening in the Lower Aare Valley in northern Switzerland that were investigated with high-resolution imaging (including X-ray computed tomography) as well as compositional and microstructural analysis. The drill cores recovered Jurassic limestones hosting palaeokarst voids infilled with blue clay. We identify this clay, based on its kaolinitic composition, as siderolithic Bolus Clay but in a rather atypical variety formed under reducing conditions. The surfaces of the palaeokarst walls show smoothly undulating as well as brecciated sections with form-fit interlocking clasts, which are the result of an *in situ* brecciation process. We discuss the origin of these particular fractures and argue that they are not related to (glacio-)tectonics or frost action. Instead, we favour an explanation by water pressure peaks that were transmitted to the void walls by the clayey karst filling, resulting in hydrofracturing. In addition to pervasive karstification and tectonic overprinting, this water pressure-driven fracturing may have assisted the deep incision of the overdeepening into the rheologically competent bedrock.

Lukas Gegg (e-mail: lukas.gegg@geo.unibe.ch), Marius W. Buechi (e-mail: marius.buechi@geo.unibe.ch) and Flavio S. Anselmetti (e-mail: flavio.anselmetti@geo.unibe.ch), Institute of Geological Sciences and Oeschger Centre for Climate Change Research, University of Bern, Baltzerstrasse 1+3, 3012 Bern, Switzerland; Andreas Ebert (e-mail: andreas.ebert@geo-ex.ch), Geo Explorers AG, Wasserturmstrasse 1, 4410 Liestal, Switzerland; Gaudenz Deplazes (e-mail: gaudenz.deplazes@nagra.ch) and Herfried Madritsch (e-mail: herfried.madritsch@nagra.ch), National Cooperative for the Disposal of Radioactive Waste (Nagra), Hardstrasse 73, 5430 Wettingen, Switzerland.

Keywords: glacial overdeepening, subglacial water pressure, pressure peak, palaeokarst, Bolus Clay

A common feature of regions currently or previously covered by ice masses are glacial overdeepenings (Linton, 1963; Preusser *et al.* 2010; Patton *et al.* 2016). These are troughs eroded deeply into the substratum by debris-laden ice and water, often several hundred metres below the surface and the local base level. They are confined at all sides, with an adverse distal slope as a distinct characteristic and therefore have strong implications for the drainage system of an overlying glacier, allowing for diverse water pathways, subglacial ponding of large water volumes and possibly partial floatation of the glacier (Cook & Swift 2012). Consequently, basal water pressures can fluctuate strongly and rapidly with peak values reaching multiples of the local ice overburden pressure (Kavanaugh & Clarke 2000; Cook *et al.* 2006; Cook & Swift 2012). Ultimately, abrupt pressure peaks can result in rupturing of the glacier bed by subglacial hydrofracturing. Such processes have been identified and described in presently and previously glaciated areas around the world (Larsen & Mangerud 1992; van der Meer *et al.* 2009), including examples dating back to the Paleozoic (Ravier *et al.* 2014). Subglacial hydrofracturing is most frequently recognized in glacial sediments; examples in solid bedrock exist but have only rarely been described (Meehan *et al.* 1997; Lloyd Davies 2004; Phillips *et al.* 2013). Due to its higher tensile strength, fracturing of bedrock requires water pressures significantly higher than those needed for fracturing of unconsolidated sediment (Phillips 1972; Cosgrove 1995; Broughton 2018), and thus its record provides an insight into extreme conditions at the glacier base.

This study presents surficial brecciation features encountered in the void walls of a sediment-filled palaeokarst from the Lower Aare Valley in the Swiss Alpine foreland. Based on high-resolution imaging together with compositional and mirostructural data, we discuss the origin of the observed structures and argue that they are possibly the result of peaks in subglacial water pressure.

Study area

Our study area is located in northern Switzerland, at the eastern margin of the WSW-ENE trending Jura mountains subdivided into the Jura fold-and-thrust belt and the northward adjacent Tabular Jura (Fig. 1). Situated about 50 km northwest of the Alpine front, the Jura mountains are built up by Mesozoic sediments deposited on an epicontinental platform. In the study area, a diverse succession of carbonates, marls and siliciclastics dating from Triassic to Jurassic is exposed, with upper Jurassic rocks (Malm) prevailing at the surface (Bitterli *et al.* 2000; Bitterli-Dreher *et al.* 2007): These are grey calcareous marl and limestone sequences of the Wildegg Fm. and overlying light-coloured micritic limestones of the Villigen Fm. In the Early Paleogene, the study area was uplifted on the forebulge of the approaching Alpine orogeny, which led to erosion and karstification of the Mesozoic carbonate plateau, while further south the Molasse Basin formed (Pfiffner 1986; Burkhard & Sommaruga 1998; Bitterli-Dreher *et al.* 2007). Karstification occurred mostly during Eocene times, when subtropical climate conditions prevailed and siderolithic deposits (formerly Bohnerz Fm.) developed from soil and limestone dissolution residues – a process that locally continued until the Miocene (Baumberger 1923; Hofmann 1991; Hofmann *et al.* 2017). These deposits consist of kaolinitic clay frequently referred to as "Bolus Clay" and may contain iron pisoliths and quartz sand (Baumberger 1923; Hofmann 1967). In Oligocene-Miocene times, Molasse sediments started to accumulate in the study area, with fine- to coarse grained clastics of the Lower Freshwater, Upper Marine, and Upper Freshwater Molasse (Berger *et al.* 2005; Bitterli-Dreher *et al.* 2007). The deposition ended in Late Miocene when the Jura fold-and-thrust belt was formed by thin-skinned deformation above an evaporitic decollement horizon (Laubscher 1962; Burkhard 1990).

During the Pleistocene, the study area was affected by a number of advances of Alpine glaciers (Graf 2009; Preusser *et al.* 2011). At the confluence area of the rivers Aare, Reuss and Limmat, the elongated Gebenstorf-Stilli Trough formed, a finger-like glacial overdeepening extending northward from the bowl-shaped Birrfeld basin (Bitterli-Dreher *et al.* 2007; Fig. 1). This 10 km-long trough has been incised into the Jura mountains by subglacial erosion, and reaches a depth of ~100 m below surface or 80 m below the lowest Pleistocene base level (300 m a.s.l.; Graf 2009). The overdeepened part of

the trough below this base level does not exceed 800 m in width (Pietsch & Jordan 2014). The contrast in cross-section from the wide Birrfeld basin in the south (Nitsche *et al.* 2001) towards the steeper and narrower Gebenstorf-Stilli Trough in the north is interpreted as a result of changing bedrock lithology from rather soft, poorly lithified Molasse sandstones towards the more resistant limestones and marls of the Jura mountains (Bitterli-Dreher *et al.* 2007). The Gebenstorf-Stilli Trough lies outside the local LGM glacier extent and was presumably eroded during the late Middle Pleistocene (Bitterli-Dreher *et al.* 2007; Graf, 2009). Today, the trough is infilled with sediment.

Erosive glacial overdeepening below the local base level requires that the adverse slope of the overdeepened basin does not exceed 1.2-1.7 the ice surface slope, as otherwise the ascending water will freeze and prevent flushing of the eroded material from the overdeepening (Hooke, 1991; Alley *et al.* 1997; Cook & Swift 2012). Hence the glacier ice must have towered considerably above the ground surface during the Gebenstorf-Stilli Trough formation, with more than 150 m of ice overlying the bedrock at the study site. The most elevated glacial deposits in the study area lie ~600 m a.s.l. (Graf *et al.* 2006; Bitterli-Dreher *et al.* 2007), corresponding to a maximum ice thickness of more than 350 m above the base of the Gebenstorf-Stilli Trough. The position of the study site, 18 km inward from the ice margin during the most extensive Möhlin Glaciation (Keller & Krayss 2010; Preusser *et al.* 2011), allows for an alternative estimation. LGM ice surface reconstructions give an average glacier thickness of ~350 m at the corresponding position (Jäckli 1970; Keller & Krayss 1993; Bini *et al.* 2009), suggesting a maximum possible ice thickness of ~450 m above the bottom of the Gebenstorf-Stilli Trough during the Pleistocene.

Methods

Core recovery and initial description

The borehole QGBR (Gegg *et al.* 2019) is located in the southern part of the Gebenstorf-Stilli Trough on the eastern bank of the river Reuss (47.4832° N, 8.2364° E; Fig. 1). It was drilled in summer 2018 in context of the Quaternary investigation program of the Swiss National Cooperative for the Disposal of Radioactive Waste (Nagra). Target of this borehole was the infill of the glacially overdeepened Gebenstorf-Stilli Trough as well as the uppermost ~10 m of the bedrock. The 10 cm diameter bedrock cores, focus of this study, were drilled by wireline using a triple-tube core barrel where the core is protected by a plastic liner. A borehole geophysical survey recorded natural gamma ray measurements and an acoustic borehole image.

The cores were analyzed at the Institute for Geological Sciences, University of Bern (IfG, UniBe) with a Geotek multi-sensor core logger (MSCL), which recorded bulk density by gamma attenuation, p-wave velocity and magnetic susceptibility in a 5 mm depth-resolution. X-ray computed tomography (CT) scans were acquired at the Institute of Forensic Medicine of UniBe and visualized using the freeware programs 3D Slicer (www.slicer.org; Kikinis *et al.* 2014) and ImageVIS 3D (www.sci.utah.edu/software/imagevis3d; Fogal & Krüger 2010). Detailed lithological and structural descriptions were carried out, including high-resolution core photography recorded with a line-scan camera.

Geochemical and mineralogical analysis

Bulk samples comprising typically ~40 g of material were collected for geochemical and mineralogical analysis. Total organic and inorganic carbon (TOC/TIC) were determined by combustion of small (few mg) sample amounts and analysis of the combustion gas in a thermal conductivity detector, and TIC was converted to $CaCO_3$ content by multiplying with a stoichiometric factor of 8.33. Mineralogical compositions were determined by x-ray diffraction, with bulk and clay mineralogy being measured in two separate approaches. For bulk mineralogy, two dried and powderized samples were spiked with Al_2O_3 powder as an internal standard and pressed into sample holders. The measurements of bulk

mineralogy were taken with an X'Pert PRO diffractometer (Cu tube, 45 kV, 40 mA, 5°–75° 2θ). The mineralogical composition was determined by a semi-automatic Rietveld refinement in HighScore Plus. Clay mineralogy was determined from a set of seven oriented samples which were prepared by pipetting a few drops of a clay suspension obtained by Atterberg separation onto glass plates. The glass plates were left to dry and then placed in an ethylene glycol atmosphere at 50 °C for at least 24 h in order to saturate swellable clay minerals within the sample. Additional oriented samples were heated to 550 °C for at least 1.5 h in order to remove kaolinite and check for the presence of chlorite. Measurements were taken with a Philips PW1830 (Cu tube, 40 kV, 30 mA, 2°–40° 2θ), and clay mineral abundances were calculated from relative peak intensities (smectite at ~5.2° 2θ, illite at ~8.8° 2θ, kaolinite at ~12.5° 2θ). We employed the 100%-approach with in-house mineral intensity factors, thus the absolute results should be treated with caution (Kahle *et al.* 2002). Trace minerals were identified with the scanning electron microscope (SEM) at IfG.

Thin section and microscopic analysis

Despite the fragility of the limestone breccia we succeeded in producing a thin section ~2.5 cm in diameter. The sample was collected from the wall of a karst void at the edge of the core at 112.59 m depth. The breccia consists of limestone fragments between 2 and 10 mm embedded in blue clay. The sample was evacuated and impregnated with epoxy before being horizontally cut and ground. Finally, the section was polished with 6 and 3 µm diamond paste. Thin-section analysis was done with an Olympus BX41 microscope with attached SC30 camera. Additionally, one bulk sample (114.98 m depth) was used for palynological screening.

Results

Stratigraphy and macroscopic description

The borehole Gebenstorf-Brüel (QGBR) terminated at a depth of 123.5 m. The Pleistocene infill of the overdeepening below an anthropogenic refill (0.0-8.0 m depth) comprises glaciofluvial gravels (8.0-23.6 m) underlain by glaciodeltaic or -lacustrine sands (23.6-108.8 m) and glacial till (108.8-111.5 m) (Fig. 2; Gegg *et al.* 2019). The bedrock was reached at 111.5 m depth and it consists of massive, light olive- to yellowish-grey micritic limestones of the Villigen Fm. of early Late Jurassic age (Oxfordian - Kimmeridgian; Bitterli *et al.* 2000). The transition from the till to the underlying bedrock is marked by a sharp decrease in the natural gamma log and magnetic susceptibility, and an increase in bulk density (Fig. 2; Gegg *et al.* 2019). Several macrofossils, possibly sponges, and dark nodules with diameters of up to 2 cm were observed, as well as frequent stylolites in varying orientations ranging from horizontal to vertical. 19 faults were logged along the 12 m bedrock core section, 15 of which could be correlated to faults detected on the acoustic image of the borehole wall allowing for orientation measurements. 14 of these faults dip towards southeast with dip angles between 5° and 31°, and one dips westwards at an angle of 17° (Fig. 2). The five non-correlated faults have dip angles between 5° and 45°.

The intervals 111.5-119.8 m and 121.0-121.5 m are penetrated by a 3D network of few millimetre- to several centimetre-wide interconnected voids identified as palaeokarst features. In the description of these features, we do not differentiate between incipient dissolution features, conduits or cavities, but simply refer to them as karst voids. The voids are filled with clayey sediment and angular limestone clasts up to fine gravel-size range. When fresh, the clayey matrix has a distinct turquoise blue colour – with some olive patches – that fades upon oxidation to blueish green and later to greenish or blueish grey (Fig. 3). The filling displays a scaly fabric (Maltman 1994) that appears strongly consolidated and breaks in shards with shiny, slickenside-like surfaces. Palynological screening did not reveal any pollen within the clay. Two different void wall morphologies can be observed: (i) smoothly undulating void walls with rough dissolution surfaces coated by a fine layer of dark brown clay (e.g. 112.5-112.9 m; Fig. 3B); and (ii) surficially brecciated void walls, with clayey filling material intruding into the fractures (e.g. 111.6-111.8 m; Fig. 3C). In several places (e.g. 111.6-111.7 m), the fragments

of the resulting limestone breccia are form-fit and interlocking, with only a narrow clay layer in between. Limestone fragments are usually limited to a few cm-wide zone around angular, fractured sections of the rock wall, no 'free-floating' clasts are observed in the larger cavities. In addition, we observe narrow (below 1 cm), sometimes branching fractures filled with angular host rock fragments and no or little clay extending from wider voids into the limestone (e.g. 116.1-116.3 and 118.4-118.8 m; Fig 3D).

Mineralogy and geochemistry of the palaeokarst filling

Bulk X-ray diffraction data of two samples (112.48 and 116.35 m depth) show that the void filling in borehole QGBR consists of ~85% clay minerals with some quartz (~10%) and calcite (up to 5%). The latter is in agreement with geochemical (TIC) data. The clay mineralogical composition is dominated by kaolinite (~60-80%) with some illite and smectite (Fig. 2, Table S1). Minor amounts of chlorite could be detected in all samples. Furthermore, few autigenic baryte crystals were identified in the SEM. TOC contents range between 0.1-0.2%.

Microstructures

Microscopic analysis of the horizontally oriented thin section at 112.59 m depth confirmed that the breccia-like material at the palaeokarst wall consists of limestone with vein-like fractures, which not always can be distinguished from narrow karst voids, filled with clayey sediment. These randomly oriented features can be as narrow as few 10s of micrometres. Their infill consists of a light, clayey matrix, few sand grains and occasionally larger clasts, which are frequently form-fit interlocking. The clasts consist of limestone not distinguishable from the host rock (Fig. 4A). The limestone bedrock contains stylolites, one of which was observed to gradually widen and transition into a lighter clay-filled fracture/void as described above (Fig. 4B). The sediment within the fractures/voids is vaguely undulatory laminated parallel to their margins, and diffuse lobate structures are observed in a ~1 mm wide fracture/void (Fig. 4C, D). Under crossed polarizers, optical anisotropy within the clay filling is evident (Fig. 4E).

Discussion

Origin of the karst void infill

A number of possible origins for the clayey material infilled into palaeokarst voids in the drill cores are tested by comparing the clay-mineral compositions to reference samples (Table S1). These include i) reworked Molasse deposits, which may show a variety of bright colours including greenish and blueish tones (Bitterli-Dreher *et al.* 2007), ii) infiltrated or injected subglacial till, and iii) pure insoluble residue from limestone dissolution. These reference materials have clay-mineral compositions dominated by illite, which agree with various analyses reported in literature (e.g. Peters 1969; Schmidt-Kaler & Salger 1986; Hofmann 1991; Schegg & Leu 1996), but are very different from the kaolinite-rich karst fillings observed in QGBR. Therefore, we rule out a Molasse as well as subglacial or pure residual origin of the karst fillings.

Illite-dominated clay mineral compositions are typical for sediments originated by prevailing physical erosion, as would be expected e.g. under a cold (Pleistocene) climate, while high abundances of kaolinite and smectite point to intense chemical weathering under warm conditions (Weaver, 1989; Chen *et al.* 2019). Palaeokarst voids in the Alpine foreland are frequently infilled with siderolithic sediments. These are of Eocene, possibly up to Miocene, age and developed from Terra Rossa-type soil formations under a subtropic climate as well as limestone dissolution residues (Baumberger 1923; Hofmann 1967; Hofmann *et al.* 2017). They consist of mostly kaolinitic Bolus Clay ("Boluston") with concentric iron oxide pisoliths ("Bohnerze") and some detrital quartz sand (Hofmann 1967; Hofmann 1991; Bitterli-Dreher *et al.* 2007). Two reference samples of Bolus Clay from borehole Bülach-1-1 (47.5427° N, 8.5204° E, 22 km E of QGBR) show clay mineral compositions of ~60% kaolinite and 40% of illite, and 5% of smectite in one of the samples (Table S1) – values that are similar to those of the karst filling in QGBR.

While typical Bolus Clay is Fe- and Al-rich and has a prominent ochre or red colour (Hofmann 1991; Bitterli-Dreher *et al.* 2007; Hofmann *et al.* 2017; see also Fig. 6), in boreholes and especially in contact with limestone, blueish or green varieties of the Bolus Clay have been encountered (Hofmann

1967; Lemcke *et al.* 1968; Matter *et al.* 1988a; Matter *et al.* 1988b). In the case of Nagra borehole WEI-1 near Weiach (18 km NE of QGBR), a downcore colour change of the Bolus Clay from 'typical' ochre towards blue-green is evident (Matter *et al.* 1988a). This evolution coincides with a change in clay mineralogy from almost pure kaolinite towards 65-70% kaolinite and 30-35% smectite (Matter *et al.* 1988a). Sediment petrography as well as clay mineral composition of the blueish Bolus Clay thus agree well with our palaeokarst fillings. We interpret the latter to consist of Bolus Clay in a blue-green variety.

The blue-green variety of the Bolus Clay is characterized by the absence of iron pisoliths in QGBR as well as in other boreholes (e.g. Lemcke 1955; Matter *et al.* 1988a). Instead, minor amounts of pyrite may be present (Lemcke 1955; Matter *et al.* 1988a). Further mineralogical data of the borehole Weiach show that goethite constitutes ~10% of the typical Bolus Clay but is not detectable within the blue-green clays (Nagra, unpubl.). The downcore development from typical ochre towards blue-green Bolus Clay therefore appears to involve the removal of iron oxides as well as the formation of smectite, likely under reducing conditions (cf. similar reduced clays in modern cave sediments of Papua New Guinea; Gillieson 1986). The smectite may act as an iron sink and could be the source of the distinct colour of the clays (Kohyama *et al.* 1973). The absence of iron minerals in the blue Bolus Clay also explains the generally low signal levels in magnetic susceptibility of the QGBR bedrock cores with only slightly increased values at larger karst voids (Fig. 2).

The lowermost two Quaternary till samples of QGBR (110.94 and 111.04 m depth) show a very similar, kaolinite-dominated clay mineral composition. This, together with the olive-blue colour of the till matrix in the lowermost 50 cm, is interpreted as a result of incorporation of Bolus Clay into the till, probably due to subglacial erosion of karstified and Bolus Clay-filled limestone, and not as a result of the mobilization and injection of till into the karst fillings. This is supported by the uniformly low carbonate content of the Bolus Clay throughout the core, which is significantly lower than in the till (up to 5% and ~35%, respectively; see Fig. 2). An insertion of till into the void filling would be visible by increased carbonate contents in the upper samples. Also, clasts of lithologies different from the karstified limestone are frequent in the till, but do not occur within the Bolus Clay.

Process of limestone brecciation

Non-sedimentary origin of the breccia. – In the palaeokarst in QGBR we observe a combination of smoothly undulating wall rock morphologies and zones of brecciated host rock as well as limestone fragments embedded in the Bolus Clay filling. While sedimentary breccias with locally derived clasts are commonly deposted in karst voids or caves (Ford & Williams 2013), the breccia in QBR cannot be explained by a simple depositional process. Here, limestone clasts are in most cases restricted to a few centimetre-wide zone around angular, fractured sections of the palaeokarst wall but neither concentrated at the bottom, nor in horizontal layers within voids, as would be expected in a sedimentary karst breccia (e.g. Guendon 1984: photo 1). 'Free-floating' isolated clasts are absent within larger voids, which indicates that the palaeokarst filling originally consisted of well-sorted pure Bolus Clay without larger fragments. The observations point towards rock-wall fracturing after infilling of the karst voids resulting in the formation of an *in situ*-breccia. We frequently observe form-fit interlocking clasts which at several places can be pieced together via 2D slices of the CT scans and fit into breakouts of the void wall (Fig. 5), which supports the idea that they are commonly derived from the rock wall that has been brecciated *in situ*. Additionally, the smoothly undulating, unbrecciated void walls are coated by a thin layer of dark brownish clay, which we interpret as a primary feature developed during karstification. This layer neither occurs on the brecciated surfaces nor on the limestone fragments embedded in the Bolus Clay, suggesting that these surfaces are younger than the unbrecciated palaeokarst walls.

Tectonic deformation. – In the 12 m long bedrock core section of QGBR a total of 19 faults were logged with remarkably uniform shallow dips towards southeast (Fig. 2). This speaks for their interpretation in the context of the Jura fold-and-thrust belt formation and is consistent with observations of outcropping corresponding limestones in the area (Madritsch 2015). This tectonic preconditioning likely facilitated the incision of the Gebenstorf-Stilli Trough and potentially played a role in the limestone brecciation observed in the drill cores. Despite the frequent occurrence of faults, the bedrock does however not appear strongly tectonized. While the karst wall surfaces are locally intensively brecciated, the larger-scale structure of the palaeokarst is intact. Evidence for major deformation of the karst walls and infill is lacking, e.g. clasts aligned in bands indicative of localized shearing (Lloyd Davies 2004). The

distribution of limestone fragments in close vicinity to the palaeokarst walls, as well as the possibility to piece adjacent clasts together, further suggests that only limited clast dislocation and Bolus Clay deformation occurred during or after the brecciation of the karst wall surfaces. Also, in contrast to the observed bedrock faults, the surficial fractures in the karst void walls show no preferred orientation (e.g. Fig. 3C).

More heavily tectonized Bolus Clay was recently recorded in Nagra borehole Bülach-1-1 (47.5427° N, 8.5204° E). It was drilled 22 km E of QGBR in a comparable position north of the Jura fold-and-thrust belt and dissected a gently dipping thrust fault branching off a complex E-W striking triangle zone (Malz *et al.* 2016; Nagra 2019). At a depth of over 500 m, Bülach-1-1 recovered Bolus-Clay-filled palaeokarst with large-scale shear planes, mirror-like faults and planar (fault-bound) contacts between rock wall and karst filling as well as large angular, but hardly form-fit limestone fragments dispersed in the Bolus Clay and partly aligned in bands (Fig. 6). In contrast, brecciated karst wall surfaces that are abundant in QGBR were rarely encountered in Bülach-1-1. Considering the deformation features in Bülach-1-1 we argue that the small-scale brecciation encountered in QGBR is not due to the comparatively mild tectonic deformations observed here. Instead, the brecciation of the karst void walls is regarded as the result of a secondary deformation process that occurred independently from tectonic structures, but not independently from the karst voids.

Glaciotectonism. – Planar shearing under overriding glacier ice can produce abundant brecciation features, as presented by Passchier *et al*. (1998) in glacial sediments from borehole CRP-1 at Roberts Ridge, Antarctica. CRP-1 recovered several brecciated intervals that contain a variety of breccia types commonly separated by sharp horizontal boundaries (Passchier *et al.* 1998). In contrast, in QGBR the style of brecciation is uniform but without a preferred orientation suggesting an undirected underlying process. The breccias in CRP-1 also span the entire core width and thus appear to be more laterally extensive than in QGBR, where the brecciation originates from the sediment-filled palaeokarst voids and does not reach further into the limestone than a few centimetres. We thus infer that the brecciation features in QGBR are not the result of glaciotectonism caused by subglacial shearing of the karstified limestone. Also, a glaciotectonic origin of the faults observed in QGBR is unlikely, as such faults would

be expected to dip steeply into the flow direction, i.e. towards north (van der Wateren, 2002; Lloyd Davies, 2004).

Frost action. – Freezing of water results in a volume increase by almost 10%, which can lead to pressure build-up and fracturing in porous rocks. Subglacial overdeepening erosion, in contrast, occurs where the glacier is warm-based, either by debris-laden ice sliding over its bed, or by subglacial meltwater (Dürst Stucki & Schlunegger 2013). Below warm-based glaciers, a water film is generated by pressure melting at the stoss side of irregularities in the bed (Weertman 1957, 1964). At the lee side of these irregularities, it can regelate. However, the regelation of water from this sub-millimetre thick film (Hallet 1979) may induce some traction and shearing of the bed, but likely not brecciation several metres below the bed surface.

With permafrost reaching as deep as 150 m into the bedrock during Pleniglacial conditions (Delisle 2003; Haeberli 2010), a temporary entire freezing of the karstified limestone in QGBR, while improbable, cannot completely be excluded. However, it is unlikely that this freezing could have resulted in frost bursting of the rock by volume expansion. To be extensive, this process demands rapid freezing so that pore pressures cannot be relieved by the migration of pore water (Matsuoka & Murton 2008) and a large number of freeze-thaw cycles (Potts 1970). Both is implausible under more than 150 m of glacier ice, where the rock is well insulated and thermally buffered. The same is true for rock fracturing by ice segregation and ice lens growth (Hallet *et al.* 1991; Murton *et al.* 2006; Matsuoka & Murton 2008) which is possible only if a threshold overburden pressure is not exceeded. This threshold overburden pressure is ~80 kPa in the idealized model case (Rempel, 2007), which corresponds to an ice thickness of less than 10 m.

Water pressure-driven brecciation. – In order to explain the surficial brecciation features in the palaeokarst walls of Gebenstorf-Brüel, we favour fracturing driven by subglacial water pressure, which may be regarded as hydrofracturing in the widest sense and at a small (centimetre-decimetre) scale. Subglacial water pressures below warm-based glaciers are known to fluctuate on a number of timescales reaching values that exceed ice overburden pressure by a factor of up to 15, even in non-overdeepened settings (Kavanaugh & Clarke 2000). The build-up of high pressures is facilitated especially if water

cannot escape from the subglacial drainage system. This is possible either if the subglacial drainage system is very inefficient or if the glacier front is frozen to the ground at the margin of the proglacial permafrost (Boulton & Caban 1995; Cook & Swift 2012). A rapid increase in subglacial water volume and pressure is possible e.g. during a jökulhlaup further up in the drainage area (Roberts *et al.* 2000; Stumm 2010). A potential source for a large meltwater outbreak could be the Birrfeld basin just few kilometres south of the drill site (Fig. 1). However, even without catastrophic events, basal water pressures have been shown to fluctuate considerably with distinct daily peaks during the melting season (Harper *et al.* 2002; Fudge *et al.* 2008). If such water pressure peaks exceed the sum of overburden and tensile strength of the bedrock – or overburden only, if pre-existing bedrock fractures can be reactivated – brittle deformation can occur, typically as (subglacial) hydrofracturing (Cosgrove 1995; Boulton & Caban 1995; Rijsdijk *et al.* 1999; Jolly & Lonergan, 2002). Subglacial hydrofracturing has been described in numerous places around the world, most frequently in glacial sediments, but it also occurs in solid bedrock, where highest water pressures are required (Meehan *et al.* 1997; Lloyd Davies 2004; Phillips *et al.* 2013; Broughton 2018). Hydrofracture systems can extend over several tens of metres (Kumpulainen 1994; Phillips *et al.* 2013; Phillips & Hughes 2014). The fractures can be several decimetres to few metres wide and are in most cases filled by sediment that is laminated parallel to the fracture walls (Larsen & Mangerud 1992; Rijsdijk *et al.* 1999; van der Meer *et al.* 2009). Complex internal structures with laminae of different grain sizes that may be graded or cross-bedded suggest that hydrofracture systems are regularly open for a prolonged time with sustained, but fluctuating water through-flow (Phillips *et al.* 2013; Phillips & Hughes 2014).

During erosion of the Gebenstorf-Stilli Trough glacier ice must have had a considerable thickness of more than 150 m of ice overlying the bedrock at the site of QGBR. This is equivalent to an overburden of ~1.4 MPa, which is already at the same magnitude as the tensile strength of limestone (Nazir *et al.* 2013; Schön 2015). However, in an interconnected drainage system up to the accumulation area of the glacier occupying the Gebenstorf-Stilli Trough located high up in the Alps, peak hydraulic heads exceeding 1000 m are possible (Kavanaugh & Clarke 2000; Beaney & Hicks 2000), e.g. during a jökulhlaup. Such a drainage system discharges a large area, which may deliver pulses of large amounts

of meltwater (Boulton & Caban 1995). The similarly thick Laurentide Ice Sheet in Canada has been shown to produce hydraulic heads and water pressures sufficient for fracturing and explosive pressure release through 100s of metres of bedrock (Christiansen *et al.* 1982; Broughton 2018). Fracturing driven by subglacial water pressure at the site of QGBR is therefore well conceivable.

The observed surficial brecciation features in the drill cores of QGBR fit some previous descriptions of glacially induced hydrofractures, e.g. by Broughton (2018), and are similar in appearance to experimental hydrofractures (Guo *et al.* 2014; Chen *et al.* 2015). Bolus Clay within the fractures (Fig. 3C) shows some microstructures indicative for viscous deformation, fluidisation, and dewatering (Maltman 1994). These are wall-parallel lamination (Fig. 4C), diffuse ball-and-pillow or drip structures (Fig. 4D; Maltman 1994; van der Meer *et al.* 2009), as well as an optical anisotropy of the clay (Fig. 4E), all of which are encountered in subglacial hydrofracures (van der Meer *et al*. 2009). However, open hydrofractures with sustained water through-flow do not seem to have existed in QGBR. Macroscopic sedimentary structures indicative for flow are lacking in the palaeokarst voids. There is further no evidence for the insertion of till or sediment-laden water into the karst filling. For example, carbonate contents in the Bolus Clay throughout the whole cored section are uniformly low with one magnitude less than in the overlying till (Fig. 2). The distribution of limestone fragments in close vicinity to the palaeokarst walls they are derived from, as well as the mosaic-like fit of adjacent clasts (Fig. 5), indicates that only limited deformation and material transport over not more than a few centimetres occurred within the karst voids during or after brecciation. Thus, classical subglacial hydrofracturing releasing pressure via fractures that allow for sustained water through-flow cannot be postulated for QGBR. Instead, a different model of pressure-driven brecciation at the site of QGBR is proposed, which may be regarded as hydrofracturing in the widest sense, i.e. a process that is driven by water pressure but does not culminate in the opening of highly permeable fractures with sustained water through-flow (Fig. 7).

During erosion of the Gebenstorf-Stilli Trough, the palaeokarst filling was in direct contact with water at the temperate glacier base, and its pressure was transferred to the porewater within the clay. In addition, pressurized water from the glacier base may have been supplied to deeper voids via joints or

faults, although we do not see evidence for this mechanism. Also, no evidence for water entering the karst system along the boundary between karst wall and clay infill occurs, neither in the shape of sedimentary structures nor as input of macroscopically or chemically identifiable till-derived material. We infer that the Bolus Clay was water-saturated and has acted as a transmitter of pressure peaks from the subglacial system – be it pure water or a wet till bed – to the karst walls. These porewater pressure peaks may have been further amplified by ground shaking due to a small earth- or ice quake as a potential side effect of the increase in basal water availability (Ozaydin & Erguvanli 1980; Mortezale & Vucetic 2013). In response to the rapid pressure increase fracturing occurred at points of weakness. These points of weakness could be stylolites (see Fig. 4B), but also pre-existing fractures that are abundant due to the local tectonic preconditioning. The observed limestone brecciation may have occurred at once or be the result of multiple brecciation events. It appears to be restricted to a small scale with centimetre- to decimetre-long fractures. Similar brittle features have been encountered at the margins of larger-scale subglacial hydrofractures in western Canada by Broughton (2018).

It is inferred that the brecciation of the limestone resulted in steep pressure gradients, i.e. considerable stress acting on the palaeokarst infill in vicinity of the newly formed fractures, and that this allowed for the semi-plastic intrusion or viscous flow of small volumes of Bolus Clay into them. Natural clays are known to display a pronounced shear-thinning or thixotropic behaviour (Coussot 1995; Fossum 2012). Laboratory experiments have shown that under stress, the viscosity of sufficiently wet clay can decrease by six orders of magnitude (Khaldoun *et al.* 2009). The remobilized clay was strongly deformed, resulting in a diffusely laminated microstructure (Fig. 4C), including ball-and-pillow/drip structures (Fig. 4D; Maltman 1994; van der Meer *et al.* 2009). Internal shearing during the intrusion led to the alignment of clay minerals within the Bolus Clay, visible as anisotropy of the material (Fig. 4E). When the deformation ceases, thixotropic materials recover and their viscosity increases again (Barnes 1997). The deformation and re-solidification under high pressures is assumed to be the reason for the consolidated appearance of the karst filling that approaches a scaly fabric (Maltman 1994). Some fractures (Fig. 3D) apparently were not infilled with clay and remained partly

open, containing only some limestone fragments; these could however be washed out by the drilling fluid.

Palaeokarst substratum and subglacial hydrology

Karstified bedrock can have a strong influence on the drainage network of an overriding glacier. It is usually highly permeable, thus subglacial water can enter the subsurface karst network and be efficiently drained from the glacier base (Smart 1983, 2004). The result can be a warm-based but largely unlubricated glacier whose sliding velocity and therefore erosional activity is greatly reduced (Smart 1983; Steinemann *et al.* 2020). The observations on our drill cores, however, show that this was not the case at the site of QGBR. The clayey pre-Pleistocene filling was obviously not flushed out of the palaeokarst system by subglacial water draining into it. There is also no evidence for any input of subglacial sediment into the Bolus Clay. This shows that the palaeokarst at our study site was effectively sealed and deactivated by cohesive clay-sized sediment. Moreover, the inferred brecciation of the wall rock under water pressure peaks indicates that the karst void filling withstood even highest water pressures. Thus, a karstified and sediment-infilled substratum does not necessarily have a distinct effect on the hydrology of an overriding glacier when compared with an unkarstified one.

Conclusions

We encountered extensive palaeokarst voids within Upper Jurassic limestone underlying a glacial overdeepening in the borehole QGBR. The palaeokarst is infilled and sealed by clayey sediment with a prominent blue colour. Based on its kaolinitic composition, we identified it as a variety of siderolithic Bolus Clay of presumably Eocene age. This variety is characterized by a significant smectite content and the absence of iron oxides, and likely developed under reducing conditions.

We infer that the karstified and brecciated limestones recovered in QGBR depict an interaction between a glacier and its subglacial drainage system. The brecciation occurred *in situ* at the boundary between limestone and karst filling. We interpret that it is unlikely the result of (glacio-)tectonic deformation or frost action but was caused by peaks in subglacial water pressure. We further suggest that the karst void filling acted as a pressure transducer from the subglacial drainage system to the void wall, where small-scale rock failures occurred at points of weakness.

In summary, the bedrock in QGBR was weakened by pervasive palaeokarst and abundant tectonic faults, which likely favoured the deep erosion of the Gebenstorf-Stilli Trough into otherwise competent bedrock. The inferred water-pressure driven fracturing of the karstified limestone below the overriding glacier may have been an additional factor facilitating erosion of the subglacial overdeepening.

Acknowledgements. – This study was supported by the Swiss National Cooperative for the Disposal of Radioactive Waste (Nagra). We would also like to kindly thank A. Berger (IfG, UniBe, SEM scanning), M. Filipponi (Nagra, discussion of karst aspects), L. Gregorczyk (Geo Explorers AG, assistance with structural core logging), M. Knipping (University of Hohenheim, palynological screening), J. Krbanjevic (IfG, UniBe, geochemical analysis), N. Lötscher (IfG, UniBe, thin section preparation), and N. Schwendener (Institute of Forensic Medicine, UniBe, CT scanning). This work further benefited from the constructive recommendations of editor J. A. Piotrowski and valuable comments of E. Ravier (University of Le Mans) and a second anonymous reviewer.

Author contributions. – Macroscopic core description was undertaken by LG, MWB and AE (structural core logging). LG performed the principal laboratory analyses and data interpretation. LG wrote the manuscript and prepared the figures; all authors contributed to editing the manuscript. The research project was planned and supervised by MWB, GD, HM and FSA.

The data that support the findings of this study are available from the corresponding author upon reasonable request.

References

Alley, R., Cuffey, K., Evenson, E., Strasser, J., Lawson, D. & Larson, G. 1997: How glaciers entrain and transport basal sediment: physical constraints. *Quaternary Science Reviews 16*, 1017-1038.

Barnes, H. A. 1997: Thixotropy – a review. *Journal of Non-Newtonian Fluid Mechanics 70*, 1-33.

Baumberger, E. 1923: Bohnerz I. Die Vorkommen im Juragebirge. *Beiträge zur Geologie der Schweiz, Geotechnische Serie 13*, 5-154.

Beaney, C. L. & Hicks, F. E. 2000: Hydraulic modelling of subglacial tunnel channels, south-east Alberta, Canada. *Hydrological Processes 14*, 2545-2557.

Berger, J.-P., Reichenbacher, B., Becker, D., Grimm, M., Grimm, K., Picot, L., Storni, A., Pirkenseer, C., Derer, C. & Schaefer, A. 2005: Palaeogeography of the upper Rhine Graben (URG) and the Swiss Molasse basin (SMB) from Eocene to Pliocene. *International Journal of Earth Sciences 94*, 697-710.

Bini, A., Buoncristiani, J., Couterrand, S., Ellwanger, D., Felber, M., Florineth, D., Graf, H., Keller, O., Kelly, M. & Schlüchter, C. 2009: *Die Schweiz während des letzteiszeitlichen Maximums (LGM) 1:500.000*. Bundesamt für Landestopographie swisstopo, Wabern.

Bitterli-Dreher, P., Graf, H., Naef, H., Diebold, P., Matousek, F., Burger, H. & Pauli-Gabi, T. 2007: *Geologischer Atlas der Schweiz 1 . 25.000. Blatt 1070 Baden. Erläuterungen*. 152 pp. Bundesamt für Landestopographie swisstopo, Wabern.

Bitterli, T., Graf, H., Matousek, F. & Wanner, M. 2000: *Geologischer Atlas der Schweiz 1 . 25.000. Blatt 1050 Zurzach. Erläuterungen*. 89 pp. Bundesamt für Landestopographie swisstopo, Wabern.

Boulton, G. & Caban, P. 1995: Groundwater flow beneath ice sheets: Part II—Its impact on glacier tectonic structures and moraine formation. *Quaternary Science Reviews 14*, 563-587.

Broughton, P. L. 2018: Subglacial blowouts in western Canada: insights into extreme meltwater pressures and hydrofracturing. *Boreas 47*, 326-346.

Buechi, M. W., Frank, S. M., Graf, H. R., Menzies, J. & Anselmetti, F. S. 2017: Subglacial emplacement of tills and meltwater deposits at the base of overdeepened bedrock troughs. *Sedimentology 64*, 658-685.

Burkhard, M. 1990: Aspects of the large-scale Miocene deformation in the most external part of the Swiss Alps (sub-Alpine molasse to Jura fold belt). *Eclogae Geologicae Helvetiae 83*, 559-583.

Burkhard, M. & Sommaruga, A. 1998: Evolution of the western Swiss Molasse basin: structural relations with the Alps and the Jura belt. *Geological Society, London, Special Publications 134*, 279-298.

Chen, D., Pan, B., Ma, J., Hu, X., Geng, H. & Pang, H. 2019: Paleoclimatic record from the clay mineralogy of Quaternary sediments of drill core DWJ from Jiudong subbasin (western Hexi Corridor), NW China. *Quaternary Research 93*, 124-138.

Chen, Y., Nagaya, Y. & Ishida, T. 2015: Observations of fractures induced by hydraulic fracturing in anisotropic granite. *Rock Mechanics and Rock Engineering 48*, 1455-1461.

Christiansen, E., Gendzwill, D. & Meneley, W. 1982: Howe Lake: a hydrodynamic blowout structure. *Canadian Journal of Earth Sciences 19*, 1122-1139.

Commission for the Geological Map of the World, Asch, K. & Bellenberg, S. 2005: *The 1: 5 million international geological map of Europe and adjacent areas (IGME 5000)*. Bundesanstalt für Geowissenschaften und Rohstoffe, Hannover.

Cook, S. J. & Swift, D. A. 2012: Subglacial basins: Their origin and importance in glacial systems and landscapes. *Earth-Science Reviews 115*, 332-372.

Cook, S. J., Waller, R. I. & Knight, P. G. 2006: Glaciohydraulic supercooling: the process and its significance. *Progress in Physical Geography 30*, 577-588.

Cosgrove, J. 1995: The expression of hydraulic fracturing in rocks and sediments. *Geological Society, London, Special Publications 92*, 187-196.

Coussot, P. 1995: Structural similarity and transition from Newtonian to non-Newtonian behavior for clay-water suspensions. *Physical Review Letters 74*, 3971.

Delisle, G., Caspers, G. & Freund, H. 2003: Permafrost in north-central Europe during the Weichselian: how deep? *Proceedings of the Eighth International Conference on Permafrost 2003,* 187-191.

Dürst Stucki, M. & Schlunegger, F. 2013: Identification of erosional mechanisms during past glaciations based on a bedrock surface model of the central European Alps. *Earth and Planetary Science Letters 384*, 57-70.

Fogal, T. & Krüger, J. H. 2010: Tuvok, an Architecture for Large Scale Volume Rendering. *Vision, Modeling and Visualization 10,* 139-146.

Ford, D. & Williams, P. D. 2007: Cave interior deposits. *In* Ford, D. & Williams, P. D. (eds.): *Karst hydrogeology and geomorphology*, 271-321. John Wiley & Sons, Chichester.

Fossum, J. 2012: Flow of clays. *The European Physical Journal Special Topics 204*, 41-56.

Fudge, T., Humphrey, N. F., Harper, J. T. & Pfeffer, W. T. 2008: Diurnal fluctuations in borehole water levels: configuration of the drainage system beneath Bench Glacier, Alaska, USA. *Journal of Glaciology 54*, 297-306.

Gegg, L., Kuster, A. M., Deplazes, G., Madritsch, H. & Buechi, M. W. 2019: Quaternary Borehole QBO Gebenstorf-Brüel (QGBR) Data Report. *Nagra Arbeitsbericht NAB 19-02*, 8 pp.

Gillieson, D. 1986: Cave sedimentation in the New Guinea highlands. *Earth Surface Processes and Landforms 11*, 533-543.

Graf, H. R. 2009: *Stratigraphie von Mittel-und Spätpleistozän in der Nordschweiz*. 198 pp. Bundesamt für Landestopographie, Wabern.

Graf, H., Bitterli-Dreher, P., Burger, H., Bitterli, T., Diebold, P. & Naef, H. 2006: *Geologischer Atlas der Schweiz 1: 25'000, Blatt 1070 Baden*. Bundesamt für Landestopografie swisstopo, Wabern.

Guendon, J.-L. 1984: Les paléokarsts des Alpes occidentales du Trias à l'Éocène. *Karstologia 4*, 2-10.

Guo, T., Zhang, S., Qu, Z., Zhou, T., Xiao, Y. & Gao, J. 2014: Experimental study of hydraulic fracturing for shale by stimulated reservoir volume. *Fuel 128*, 373-380.

Haeberli, W. 2010: Glaciological conditions in northern Switzerland during recent Ice Ages. *Nagra Arbeitsbericht NAB 10-18*, 28 pp.

Hallet, B. 1979: Subglacial regelation water film. *Journal of Glaciology 23*, 321-334.

Hallet, B., Walder, J. & Stubbs, C. 1991: Weathering by segregation ice growth in microcracks at sustained subzero temperatures: Verification from an experimental study using acoustic emissions. *Permafrost and Periglacial Processes 2*, 283-300.

Harper, J. T., Humphrey, N. F. & Greenwood, M. C. 2002: Basal conditions and glacier motion during the winter/spring transition, Worthington Glacier, Alaska, USA. *Journal of Glaciology 48*, 42-50.

Hofmann, F. 1967: Über die Tertiärbildungen im Kanton Schaffhausen. *Mitteilungen der Naturforschenden Gesellschaft Schaffhausen 28*, 171-211.

Hofmann, F. 1991: Neue Befunde zur Geologie, zur Lagerstättenkunde und zum historischen Abbau der Bohnerze und Bolustone der Region Schaffhausen. *Mitteilungen der Naturforschenden Gesellschaft Schaffhausen 36*, 45-81.

Hofmann, F., Reichenbacher, B. & Farley, K. A. 2017: Evidence for> 5 Ma paleo-exposure of an Eocene–Miocene paleosol of the Bohnerz Formation, Switzerland. *Earth and Planetary Science Letters 465*, 168-175.

Hooke, R. L. 1991: Positive feedbacks associated with erosion of glacial cirques and overdeepenings. *Geological Society of America Bulletin 103*, 1104-1108.

Jäckli, H. 1970: *Die Schweiz zur letzten Eiszeit 1:550.000*. Eidgenössische Landestopographie, Wabern.

Jolly, R. J. & Lonergan, L., 2002: Mechanisms and controls on the formation of sand intrusions. *Journal of the Geological Society 159*, 605-617.

Kahle, M., Kleber, M. & Jahn, R. 2002: Review of XRD-based quantitative analyses of clay minerals in soils: the suitability of mineral intensity factors. *Geoderma 109*, 191-205.

Kavanaugh, J. L. & Clarke, G. K. 2000: Evidence for extreme pressure pulses in the subglacial water system. *Journal of Glaciology 46*, 206-212.

Keller, O. & Krayss, E. 1993: The Rhine-Linth Glacier in the upper Wurm: a model of the last Alpine glaciation. *Quaternary International 18*, 15-27.

Keller, O. & Krayss, E. 2010: Mittel-und spätpleistozäne Stratigraphie und Morphogenese in Schlüsselregionen der Nordschweiz. *E&G Quaternary Science Journal 59*, 88-119.

Khaldoun, A., Moller, P., Fall, A., Wegdam, G., De Leeuw, B., Méheust, Y., Fossum, J. O.& Bonn, D. 2009: Quick clay and landslides of clayey soils. *Physical Review Letters 103*, 188301, DOI: 10.1103/PhysRevLett.103.188301.

Kikinis, R., Pieper, S. D. & Vosburgh, K. G. 2014: 3D Slicer: a platform for subject-specific image analysis, visualization, and clinical support. *In* Jolesz, F. A. (ed.): *Intraoperative imaging and image-guided therapy*, 277-289. Springer, New York.

Kohyama, N., Shimoda, S. & Sudo, T. 1973: Iron-rich saponite (ferrous and ferric forms). *Clays and Clay Minerals 21*, 229-237.

Kumpulainen, R. A. 1994: Fissure-fill and tunnel-fill sediments: expressions of permafrost and increased hydrostatic pressure. *Journal of Quaternary Science 9*, 59-72.

Larsen, E. & Mangerud, J. 1992: Subglacially formed clastic dikes. *Sveriges Geologiska Undersökning 81*, 163-170.

Laubscher, H. P. 1962: Die Zweiphasenhypothese der Jurafaltung. *Eclogae Geologicae Helvetiae 55*, 1-22.

Lemcke, K. 1955: Die Fazies des Jura der Bohrung Scherstetten 1. *Geologica Bavarica 24*, 52-65.

Lemcke, K., Büchi, U. & Wiener, G. 1968: Einige Ergebnisse der Erdölexploration auf die mittelländische Molasse der Zentralschweiz. *Bulletin der schweizerischen Vereinigung Petroleum-Geologen und -Ingenieure 35*, 15-34.

Linton, D. L. 1963: The forms of glacial erosion. *Institute of British Geographers Transactions and Papers 33*, 1-28.

Lloyd Davies, M. 2004: A polar paradise: The glaciation of South Victoria Land, Antarctica. *Academisch Proefschrift UvA Amsterdam*, 304 pp.

Madritsch, H. 2015: Outcrop-scale fracture systems in the Alpine foreland of central northern Switzerland: Kinematics and tectonic context. *Swiss Journal of Geosciences 108*, 155-181.

Maltman, A. 1994: Deformation structures preserved in rocks. *In* Maltman, A. (ed.): *The geological deformation of sediments*, 261-307. Springer Science+Business Media, Dordrecht.

Malz, A., Madritsch, H., Meier, B. & Kley, J. 2016: An unusual triangle zone in the external northern Alpine foreland (Switzerland): Structural inheritance, kinematics and implications for the development of the adjacent Jura fold-and-thrust belt. *Tectonophysics 670*, 127–143.

Matsuoka, N. & Murton, J. 2008: Frost weathering: recent advances and future directions. *Permafrost and Periglacial Processes 19*, 195-210.

Matter, A., Peters, T., Bläsi, H., Meier, J., Ischi, H. & Meyer, C. 1988a: Sondierbohrung Weiach. Geologie. *Geologischer Bericht der Landeshydrologie und -geologie 6*, 438 pp.

Matter, A., Peters, T., Bläsi, H., Schenker, F. & Weiss, H. 1988b: Sondierbohrung Schafisheim. Geologie. *Geologischer Bericht der Landeshydrologie und -geologie 8*, 321 pp.

Meehan, R. T., Warren, W. P. & Gallagher, C. J. 1997: The sedimentology of a Late Pleistocene drumlin near Kingscourt, Ireland. *Sedimentary Geology 111*, 91-105.

van der Meer, J. J., Kjær, K. H., Krüger, J., Rabassa, J. & Kilfeather, A. 2009: Under pressure: clastic dykes in glacial settings. *Quaternary Science Reviews 28*, 708-720.

Mortezale, A. R. & Vucetic, M. 2013: Effect of frequency and vertical stress on cyclic degradation and pore water pressure in clay in the NGI simple shear device. *Journal of Geotechnical and Geoenvironmental Engineering 139*, 1727-1737.

Murton, J. B., Peterson, R. & Ozouf, J.-C. 2006: Bedrock fracture by ice segregation in cold regions. *Science 314*, 1127-1129.

Nagra 2019: Preliminary horizon and structure mapping of the Nagra 3D seismics NL-16 (Nördlich Lägern) in time domain. *Nagra Arbeitsbericht NAB 18-35*, 63 pp.

Nazir, R., Momeni, E., Armaghani, D. J. & Amin, M. M. 2013: Correlation between unconfined compressive strength and indirect tensile strength of limestone rock samples. *Electronic Journal of Geotechnical Engineering 18*, 1737-1746.

Nitsche, F., Monin, G., Marillier, F., Graf, H. & Ansorge, J. 2001: Reflection seismic study of Cenozoic sediments in an overdeepened valley of northern Switzerland: the Birrfeld area. *Eclogae Geologicae Helvetiae 94*, 363-371.

Ozaydin, K. & Erguvanli, A. 1980: The generation of pore pressures in clayey soils during earthquakes. *Proceedings of the 7th World Conference on Earthquake Engineering*, 326-330.

Passchier, S., Wilson, T. & Paulsen, T. 1998: Origin of Breccias in the CRP-1 Core. *Terra Antartica 5*, 401-409.

Patton, H., Swift, D., Clark, C., Livingstone, S. J. & Cook, S. J. 2016: Distribution and characteristics of overdeepenings beneath the Greenland and Antarctic ice sheets: Implications for overdeepening origin and evolution. *Quaternary Science Reviews 148*, 128-145.

Peters, T. 1969: Tonmineralogie einiger Glazialablagerungen im schweizerischen Mittelland. *Ecologae Geologicae Helvetiae 62*, 517-525.

Pfiffner, O. A. 1986: Evolution of the north Alpine foreland basin in the Central Alps. *Special Publications of the International Association of Sedimentologists 8*, 219-228.

Phillips, W. J. 1972: Hydraulic fracturing and mineralization. *Journal of the Geological Society 128*, 337-359.

Phillips, E., Everest, J. & Reeves, H. 2013: Micromorphological evidence for subglacial multiphase sedimentation and deformation during overpressurized fluid flow associated with hydrofracturing. *Boreas 42*, 395-427.

Phillips, E. & Hughes, L. 2014: Hydrofracturing in response to the development of an overpressurised subglacial meltwater system during drumlin formation: an example from Anglesey, NW Wales. *Proceedings of the Geologists' Association 125*, 296-311.

Pietsch, J. & Jordan, P. 2014: Digitales Höhenmodell Basis Quartär der Nordschweiz - Version 2014 und ausgewählte Auswertungen. *Nagra Arbeitsbericht NAB 14-02*, 69 pp.

Potts, A. S. 1970: Frost action in rocks: some experimental data. *Transactions of the Institute of British Geographers 49*, 109-124.

Preusser, F., Graf, H. R., Keller, O., Krayss, E. & Schlüchter, C. 2011: Quaternary glaciation history of northern Switzerland. *E&G Quaternary Science Journal 60*, 282-305.

Preusser, F., Reitner, J. M. & Schlüchter, C. 2010: Distribution, geometry, age and origin of overdeepened valleys and basins in the Alps and their foreland. *Swiss Journal of Geosciences 103*, 407-426.

Ravier, E., Buoncristiani, J.-F., Guiraud, M., Menzies, J., Clerc, S., Goupy, B. & Portier, E. 2014: Porewater pressure control on subglacial soft sediment remobilization and tunnel valley formation: A case study from the Alnif tunnel valley (Morocco). *Sedimentary Geology 304*, 71-95.

Rempel, A. 2007: Formation of ice lenses and frost heave. *Journal of Geophysical Research 112*, DOI: 10.1029/2006JF000525.

Rijsdijk, K. F., Owen, G., Warren, W. P., McCarroll, D. & van der Meer, J. J. 1999: Clastic dykes in over-consolidated tills: evidence for subglacial hydrofracturing at Killiney Bay, eastern Ireland. *Sedimentary Geology 129*, 111-126.

Roberts, M. J., Russell, A. J., Tweed, F. S. & Knudsen, Ó. 2000: Ice fracturing during jökulhlaups: implications for englacial floodwater routing and outlet development. *Earth Surface Processes and Landforms 25*, 1429-1446.

Schegg, R. & Leu, W. 1996: Clay mineral diagenesis and thermal history of the Thonex Well, Western Swiss Molasse Basin. *Clays and Clay Minerals 44*, 693-705.

Schmidt-Kaler, H. & Salger, M. 1986: Obere Süßwassermolasse (OSM) und Bunte Breccie bei Bieswang (Südliche Frankenalb): neue Kernbohrungen und sedimentpetrographische Untersuchungen. *Geologica Bavarica 89*, 219–228.

Schön, J. H. 2015: Geomechanical Properties. *In* Schön, J. H. (ed.): *Physical properties of rocks: Fundamentals and principles of petrophysics*, 269-300. Elsevier, Amsterdam.

Smart, C. 1983: The hydrology of the castleguard karst, columbia icefields, Alberta, Canada. *Arctic and Alpine Research 15*, 471-486.

Smart, C. 2004: Glacierized and glaciated karst. *In* Gunn, J. (ed.): *Encyclopedia of caves and karst science, 804-809.* Fitzroy Dearborn, New York.

Steinemann, O., Ivy-Ochs, S., Grazioli, S., Luetscher, M., Fischer, U. H., Vockenhuber, C. & Synal, H. A. 2020: Quantifying glacial erosion on a limestone bed and the relevance for landscape development in the alps. *Earth Surface Processes and Landforms,* DOI: 10.1002/esp.4812.

Stumm, D. 2010: Deep glacial erosion. Review with focus on tunnel valleys in northern Europe. *Nagra Arbeitsbericht NAB 10-33*, 74 pp.

Swisstopo 2013: *swissALTI3D*. Bundesamt für Landestopographie swisstopo, Wabern.

van der Wateren, D. M. 2002: Processes of glaciotectonism. *In* Menzies, J. (ed.): *Modern and Past Glacial Environments*, 417-443. Butterworth-Heinemann, Oxford.

Weaver, C. E. 1989: Soils and Weathering. *In* Weaver, C. E. (ed.): *Clays, muds, and shales,* 103-189. Elsevier, Amsterdam.

Weertman, J. 1957: On the sliding of glaciers. *Journal of Glaciology 3*, 33-38.

Weertman, J. 1964: The theory of glacier sliding. *Journal of Glaciology 5*, 287-303.

Figures

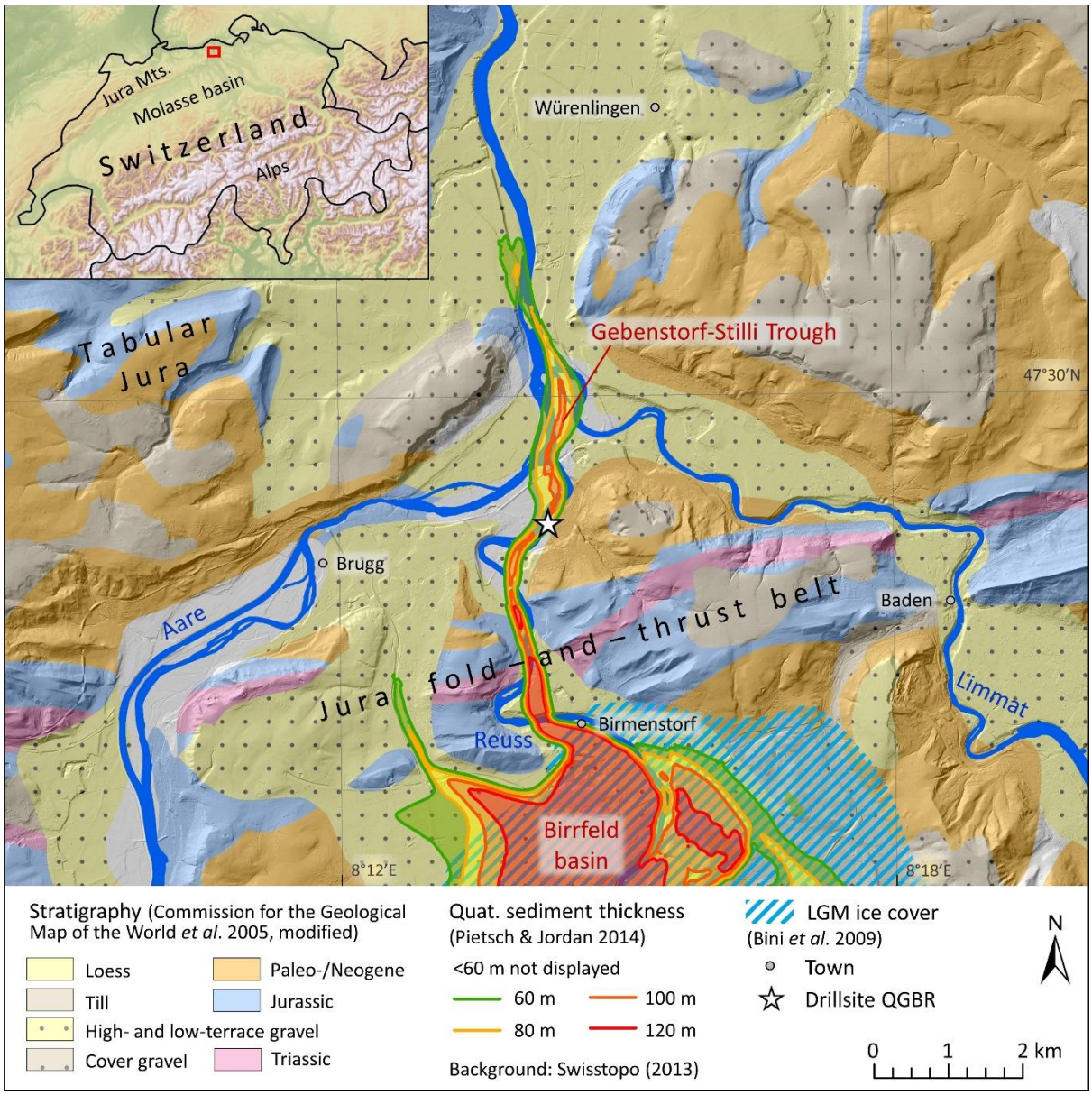

Fig. 1. Map of the study area displaying the position of the drillsite QGBR (47.4832° N, 8.2364° E), LGM ice extent, surface geology (simplified), and the position of the Gebenstorf-Stilli Trough as marked by thick Quaternary sediments. The inset on the left shows the regional geological context and the red rectangle indicates the study area at the eastern end of the Jura mountains.

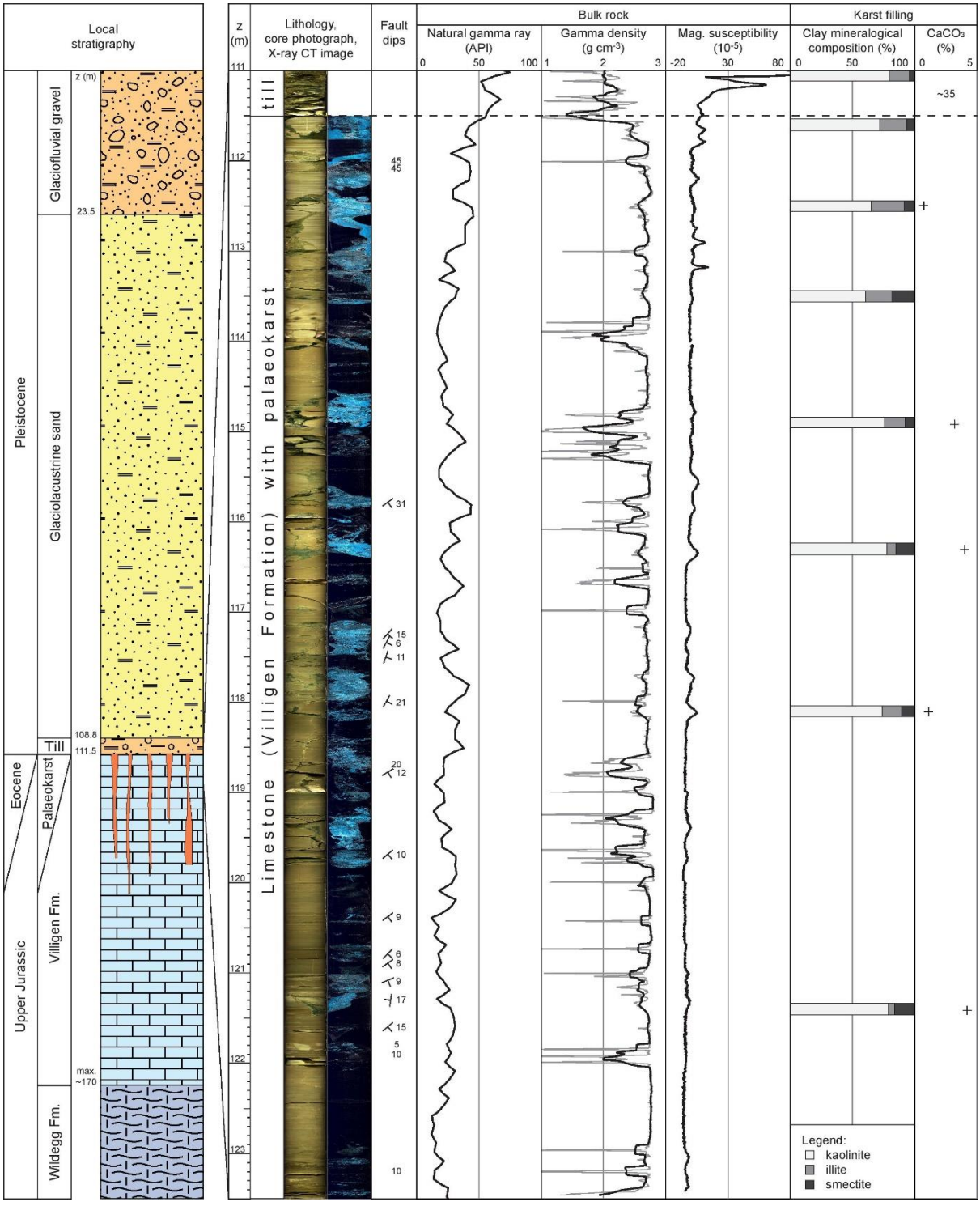

Fig. 2. Overview plot of the 12.5 m bedrock section at bottom of the borehole QGBR (total depth 123.5 m) in the local stratigraphic context. Core photograph and X-ray CT image column (low-density material (palaeokarst filling) is light blue, high-density material (limestone) is black) are horizontally stretched by a factor of ~5. Dip direction of faults is given where correlation with ABI is possible. Gamma density is displayed as 20 cm moving average (black) and raw data (grey).

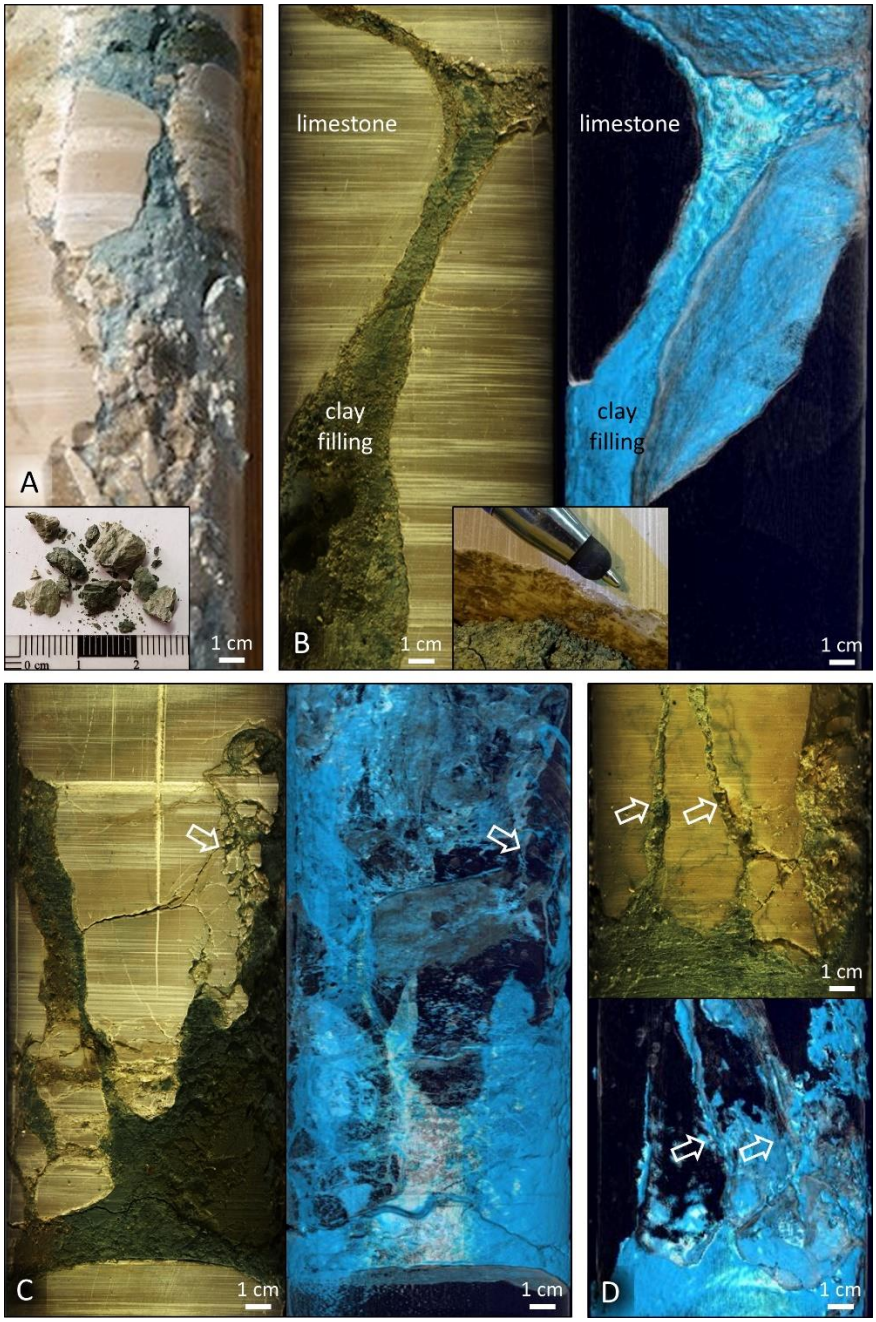

Fig. 3. Palaeokarst voids: infill and wall morphologies. Note drilling-related surface grooves on the limestone surfaces. A. Photograph of the fresh core. Note the prominent blue colour of the clayey palaeokarst filling. Inset: dried filling broken into shards. B. Smoothly undulating void walls (112.5-112.8 m depth; left: core photograph, right: CT image, low-density material (clay filling) is light blue, high-density material (limestone) is transparent/black). Note the dark clay coating on the wall surfaces (inset). C. Brecciated void wall surfaces (111.6-111.8 m depth; left: core photograph, right: CT image). D. Narrow fractures filled with angular host rock fragments but only little clay (116.2-116.4 m depth; top: core photograph, bottom: CT image).

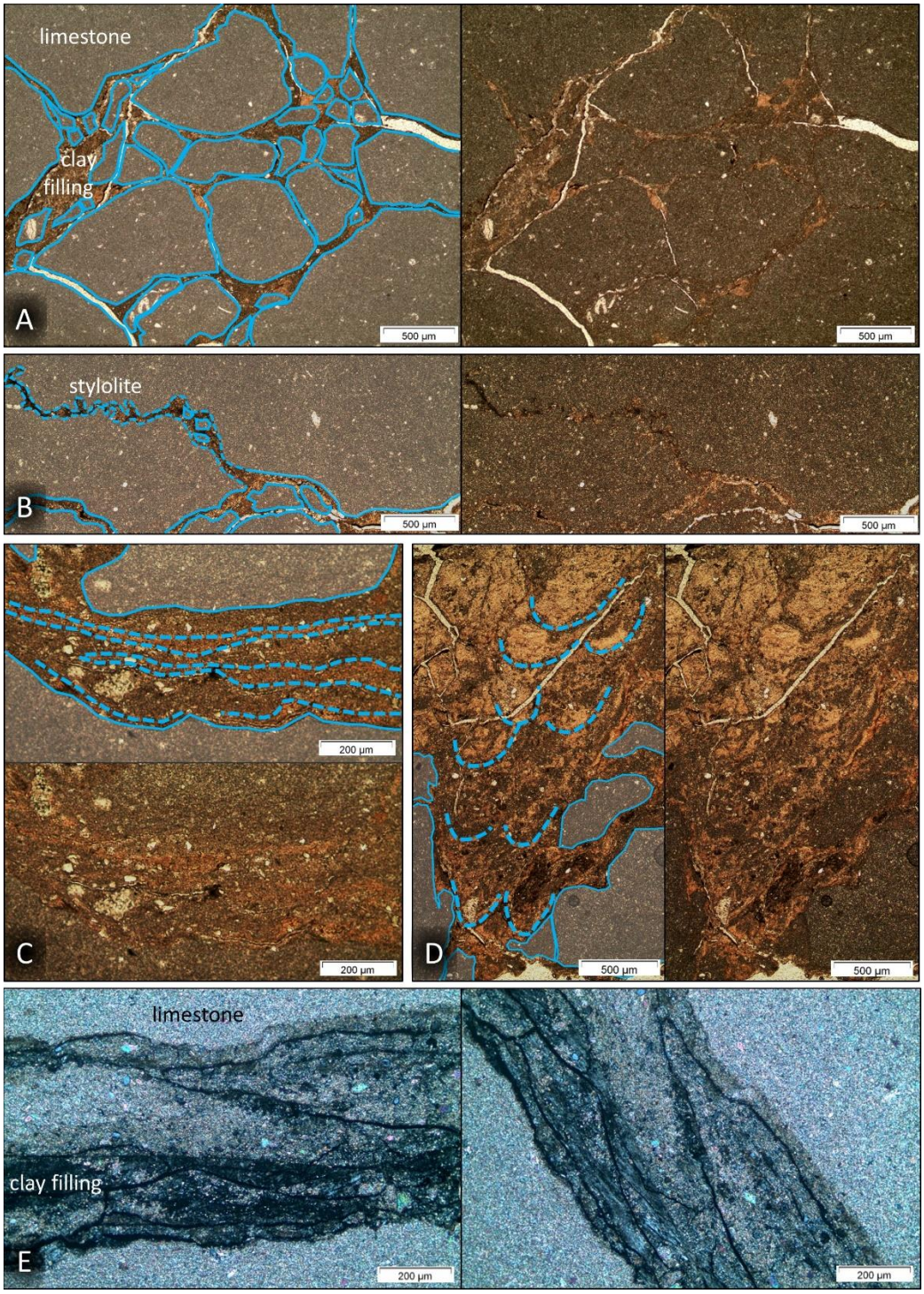

Fig. 4. Microstructures in karstified limestone of QGBR (horizontally oriented thin section at 112.59 m depth). A. Palaeokarst void/fracture infilled with interlocking limestone fragments embedded in Bolus Clay. B. Transition of stylolite (dashed) into clay-filled void/fracture. C. Diffusely laminated Bolus Clay filling of void/fracture. D. Lobate microstructures ('ball-and-pillow structures', Maltman 1994; 'drip structures', van der Meer *et al.* 2009) in the filling of a larger void/fracture. E. Optical anisotropy of the clayey infill under crossed polarizers (black lines are cracks related to the preparation process).

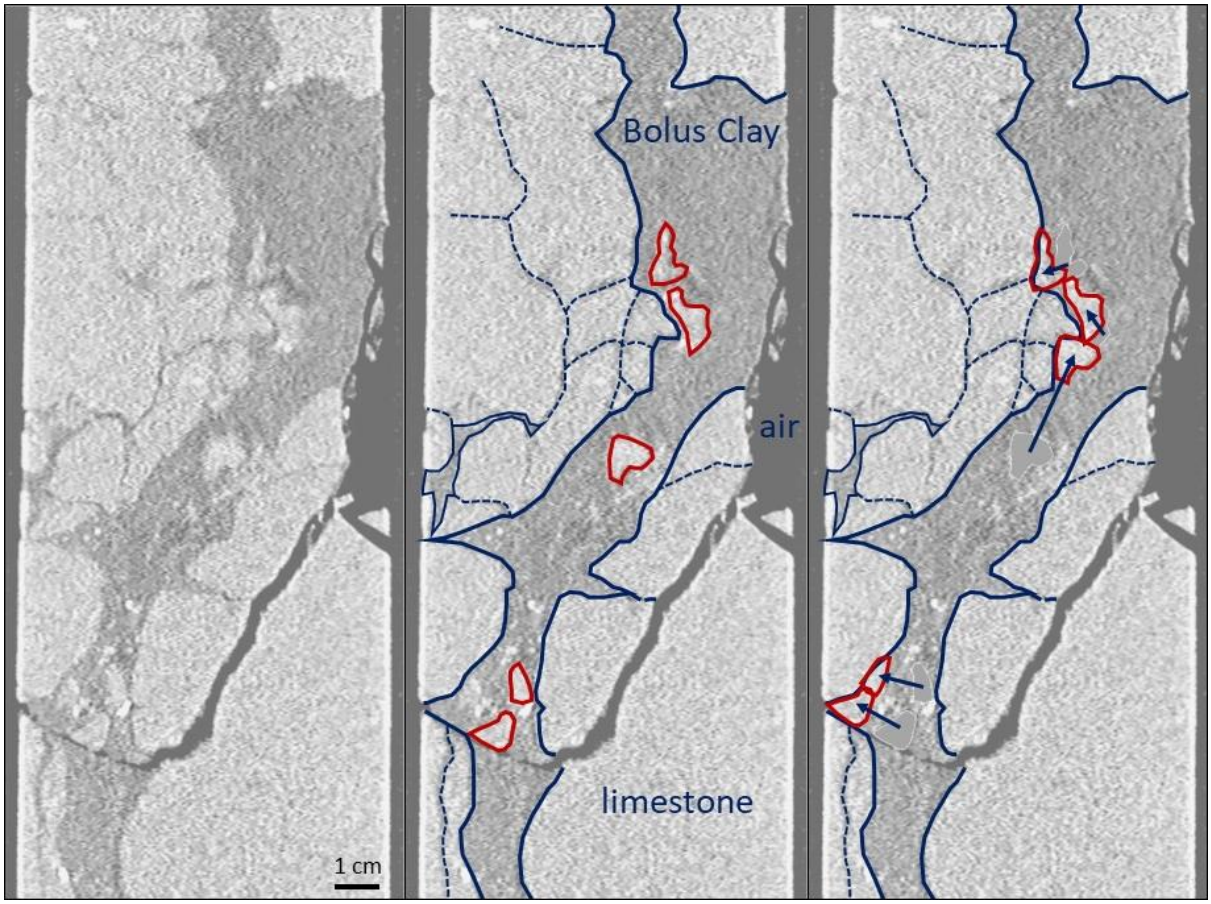

Fig. 5. Limestone with palaeokarst, vertical 2D slice of a CT scan at ~112.5 m depth (left). The limestone can be distinguished well from the palaeokarst infill (middle). Note fragments of limestone embedded within the Bolus Clay (red outline). These fragments can be pieced back together and fit into breakouts of the wall rock (right), giving an impression of the void wall prior to brecciation.

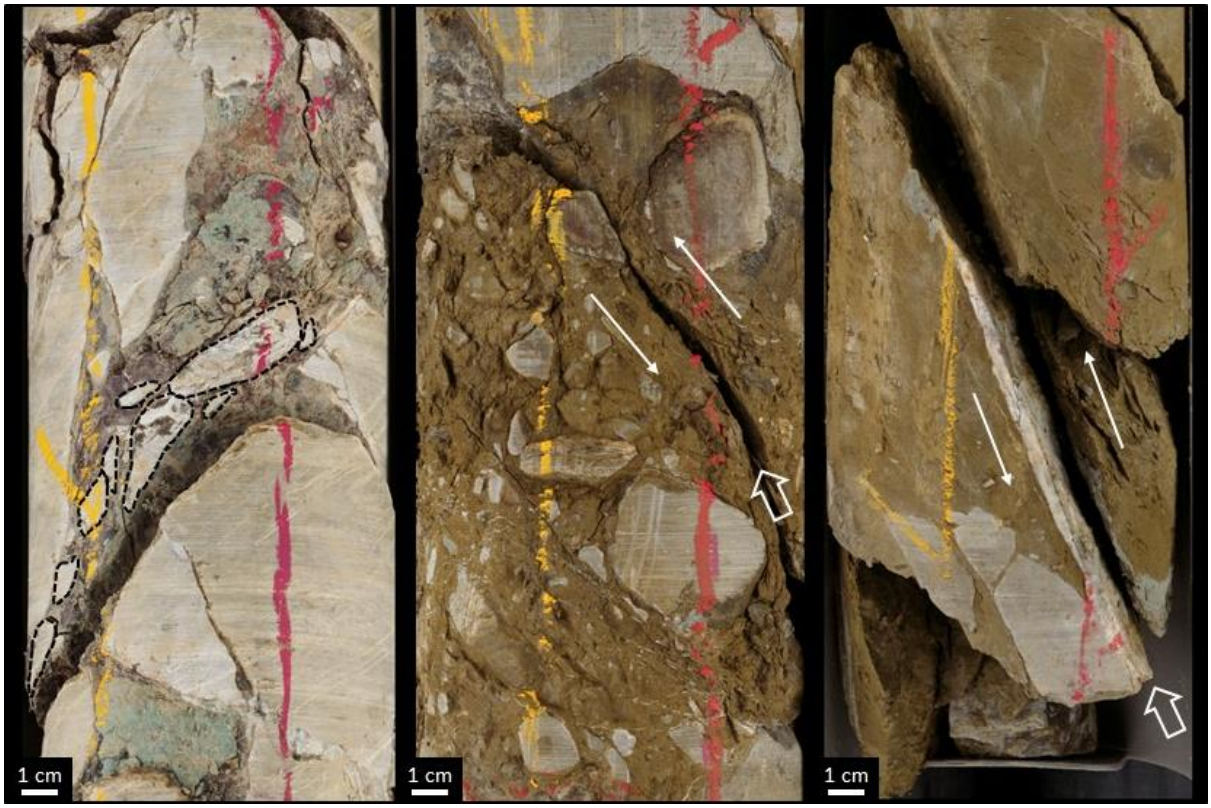

Fig. 6. Indicators of strong tectonic overprinting of karstified, Bolus Clay-filled limestone in Nagra borehole Bülach-1-1. Left: fragments aligned in discrete band indicative of shearing (541.3-541.5 m depth). Middle: Larger palaeokarst void with dispersed, non-form-fit fragments and dissected by a fault (arrow; 549.8-550.0 m). Right: Fault plane with calcite mineralization (arrow, 550.8-551.0 m). Photograph courtesy of Nagra.

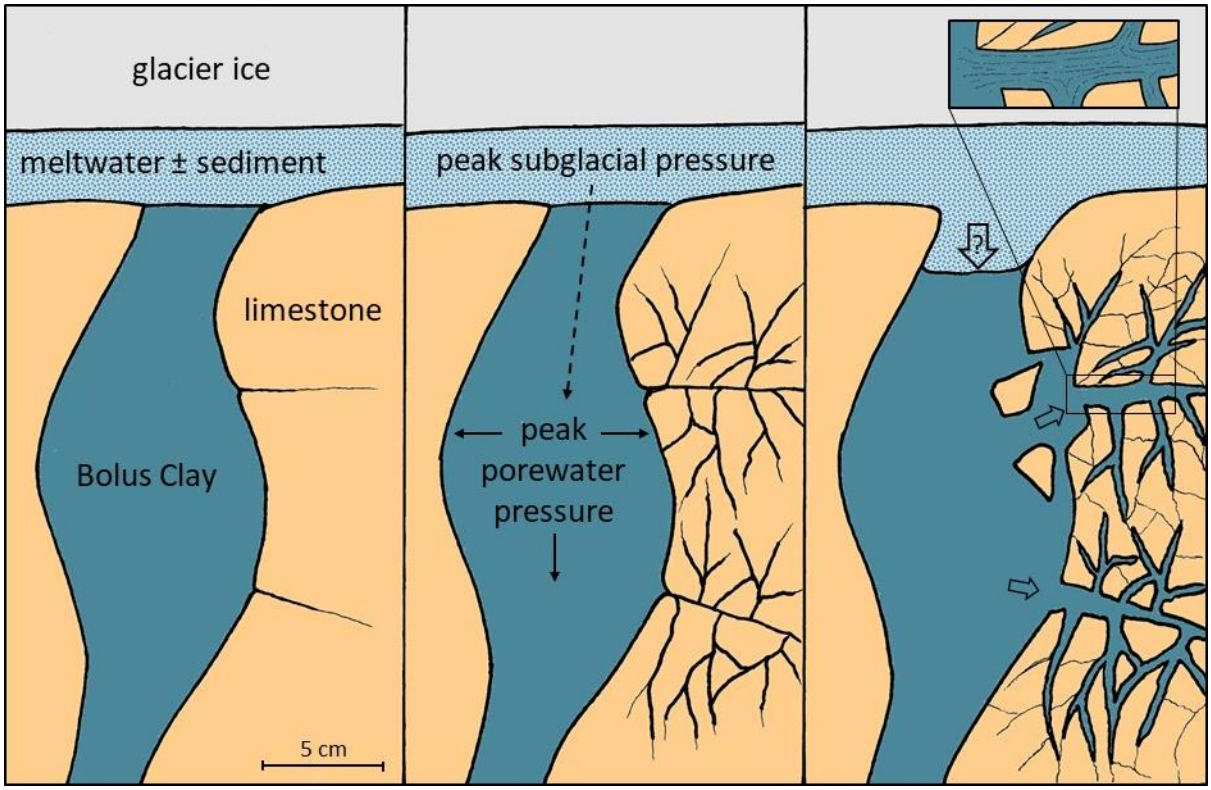

Fig. 7. Conceptual model of water pressure-driven brecciation in QGBR. The Bolus Clay filling in the palaeokarst voids was in direct contact with the subglacial drainage system of the overriding, overdeepening glacier (left). Peak subglacial water pressures were transmitted via the porewater pressure of the clay filling, to the rock wall, initiating fracturing at points of weakness (middle). Opening of short (centimetre- to decimetre-scale) fractures within the rock wall allowed for the intrusion of Bolus Clay and pressing of the karst filling into the voids (right). Strong deformation of the Bolus Clay intruding into the newly formed fractures led to a diffusely laminated microstructure (inset) as well as ball-and-pillow/drip structures and optical anisotropy.

Supporting Information

Table S1: Clay-mineral compositions determined for karst fillings in borehole QGBR as well as reference samples from QGBR, other Quaternary boreholes of the drilling campaign (QGVO = Gebenstorf-Vogelsang, 47.5952° N, 8.2382° E; QRIN = Riniken, 47.5021° N, 8.1913° E; QTRU = Trüllikon, 47.6405° N, 8.6624° E) and Nagra borehole Bülach-1-1 (Bul-1-1, 47.5427° N, 8.5204° E).

Borehole, sample depth	Kaolinite	Illite	Smectite
Karst filling			
QGBR, 111.60 m	72%	22%	6%
QGBR, 112.48 m	65%	27%	8%
QGBR, 113.53 m	61%	21%	18%
QGBR, 114.90 m	76%	17%	7%
QGBR, 116.35 m	78%	7%	15%
QGBR, 118.13 m	74%	15%	10%
QGBR, 121.42 m	79%	5%	16%
Reference samples: subglacial till			
QGBR, 108.86 m	23%	60%	17%
QGBR, 109.54 m	24%	53%	22%
QGBR, 110.94 m	76%	14%	10%
QGBR, 111.04 m	80%	16%	4%
QGVO, 64.63 m	25%	63%	11%
QRIN, 38.89 m	19%	81%	-
QRIN, 40.99 m	21%	79%	-
Reference samples: Lower Freshwater Molasse			
QTRU, 91.00 m	20%	49%	31%
QTRU, 95.00 m	24%	49%	27%
Reference sample: limestone dissolution residue (clayey coating of a fault plane)			
QGBR, 123.40 m	34%	66%	-
Reference samples: siderolithic "Bolus Clay"			
Bul-1-1, 539.00 m	56%	5%	39%
Bul-1-1, 550.30 m	60%	-	40%